LASER INTERFEROMETER GRAVITATIONAL WAVE OBSERVATORY
- LIGO -
CALIFORNIA INSTITUTE OF TECHNOLOGY
MASSACHUSETTS INSTITUTE OF TECHNOLOGY

Document Type	**LIGO-T970177-00 - D**	12/2/97

Doubly Resonant Sideband Control for LIGO

McClelland, Whitcomb, Kells, Camp

Distribution of this draft:

This is an internal working note
of the LIGO Project..

California Institute of Technology
LIGO Project - MS 51-33
Pasadena CA 91125
Phone (818) 395-2129
Fax (818) 304-9834
E-mail: info@ligo.caltech.edu

Massachusetts Institute of Technology
LIGO Project - MS 20B-145
Cambridge, MA 01239
Phone (617) 253-4824
Fax (617) 253-7014
E-mail: info@ligo.mit.edu

WWW: http://www.ligo.caltech.edu/

1 INTRODUCTION

This note advocates a change in the initial LIGO optical configuration. The authors feel the advantages of this change are sufficiently compelling that they justify its implementation and attendant schedule impact at this advanced stage in the detector design.

The new approach involves resonating the gravitational wave sensing sidebands in the arm cavities (we will refer to this configuration as Doubly Resonant Sidebands or DRSB, while the baseline configuration, which has the sidebands resonating only in the Michelson cavity, will be known as Singly Resonant Sideband or SRSB). In a nutshell, by resonating the sidebands in the arms, DRSB applies spatial and temporal filtering, thereby suppressing noise on the sidebands by a large factor, in most cases order 50. The reason DRSB is important is that, as we have learned in the last year, many of our most serious noise sources are dominated by sideband noise and/or instability. These include:

- Thermal lensing from absorption in recycling cavity causing sideband instability, power loss and “start-up” problem
- Uncertainty of recycling cavity mirror radius of curvature causing sideband instability
- RF intensity noise
- In-band frequency and intensity noise
- Beam jitter noise

Most of these noise terms can be addressed by independent measures. For example, low absorption glass and rigorous vacuum cleanliness will limit thermal lensing (bullet 1), a premode cleaner has been added to the PSL to filter the sideband RF noise (bullet 3), and sufficient LSC and ASC servo gain has been allocated to limit the couplings of frequency, intensity and jitter noise to the GW signal (bullets 4 and 5). Nevertheless, the *DRSB configuration would directly lower the sensitivity of the GW signal to all of these effects by 1 - 2 orders of magnitude*. Thus DRSB provides a more robust, stable configuration and also points the way to the advanced LIGO where additional noise suppression is mandatory.

In this document we give a summary of the advantages and disadvantages of adopting DRSB, and then proceed to a fuller discussion of the issues.

2 SUMMARY OF ADVANTAGES / DISADVANTAGES OF DRSB

Table 1: Modulation Scheme Comparison

	DRSB	SRSB
DRSB Advantages		
Spatial Filtering - Tolerance to Input Power, ROC, at 10% loss in sens		
Maximum power input (6 W nominal)	> 60 W	7 W
Maximum ROC error in RM	> 50 %	6 %
Length Sensing and Control		
Change in sideband gain for above power and ROC tolerances	1 %	40 %
Change in sideband gain for lock acquisition (cold) mode	1 %	factor 25
Temporal Filtering - Coupling of Laser Fluctuations to GW signal		
Frequency Noise	1	50
Intensity Noise	1	50
Beam Jitter Noise	1	50
RF Intensity Noise	1	50
DRSB Disadvantages		
DC Arm length control	0.3 mm	-
Required sidebands	19.7 MHz, 502.35MHz	25 MHz
Schedule impact on ISC	~ 3 months (?)	-

The most serious technical problem in the implementation of DRSB is control of the arm cavity DC length at the level of 0.3 mm. We have no experience in DC control of a 4 km cavity at this level; however we find an adequate error signal for the DC length control is available. We also have no experience with sideband generation and detection at 500 MHz, but the technology for this is available. These problems are discussed in later sections.

§2 The SRSB Technique

§2.1 Overview

Fig.1 shows a schematic layout of the LIGO interferometer. It is a standard arm cavity power recycling Michelson interferometer, frontally modulated. The Michelson asymmetry, $\delta = (l_P - l_I)$, is adjusted to maximize the output of the rf sidebands at the asymmetric port for gw signal extraction. Four lengths need to be controlled about their nominal lengths: the common mode lengths, $L+ = (L_P + L_I)$ and $l+ = (l_P + l_I)$; and the differential mode lengths, $L- = (L_P - L_I)$ and $l- = \delta$.

Fig. 1 also shows the 3 standard ports at which control signals, either in phase (I) or 90^o out of phase (Q) with the phase modulation can be extracted: port 1, light reflected off the power recycling mirror, mirror M1, can be extracted from the Faraday isolator; port 2 is a reflection from the beam splitter; and port 3 is the Michelson antisymmetric port. Ideally, we would like to extract 4 independent error signals. In practice, each output responds predominantly to a specific length change (either common or differential), but has a small component of the other (common/ differential resp.) component in it, thus imposing a locking hierarchy.

For the SRSB method, the nominal lengths are chosen so that when the carrier resonates in the arms and the power recycling cavity, PRC, the sidebands resonate only in the PRC. This is achieved when $L+/2 \sim (m+ 1/2)c/2f_{mod}$ and $l+ \sim (n + 1/2)c/2f_{mod}$, m and n integers. The reflectivity of the PR mirror is chosen for optimum carrier coupling. Under these conditions, after demodulation at the rf frequency, the in phase signals at ports 1 and 2 respond mainly to the arm cavity common mode length fluctuation; the quad phase at port 2 mainly to Michelson differential motions; and the quad phase at port 3 to arm cavity differential motions. Michelson common mode changes are not dominant at any port and therefore must be controlled after locking the arm cavity common mode. The matrix of discriminants is given in Table 2.

§2.2 Stability Requirements

Extensive analysis has been carried out on this arrangement. How well these length fluctuations can be controlled along with the level of matching of the interferometer arms, sets limitations on the stability of the input light and of the rf source.

Table 3 summarizes the requirements for LIGO to achieve a sensitivity of 10^{-20} m at 100 Hz. Fluctuations in the signals arise due to beating of the rf sidebands with audio (noise) sidebands of the carrier and the beating of carrier light with audio sidebands on the rf sidebands. As the carrier light is resonant in both the PRC and the arm cavities, it is propagating in a stable mode, coupled cavity with a linewidth of less than 1.5 Hz! As a result audio sidebands on the carrier above 1.5 Hz are stripped off. The rf sidebands however are not resonant in the arm cavities. Therefore they propagate only in the PRC, which has a pole frequency at some 75 kHz. Hence it is the audio sidebands on the rf sidebands beating with the carrier light which dominant the noise budget.

Columns 1 and 2 refer to the laser frequency and amplitude noise. Extra noise is added to the rf sidebands, by the rf oscillator during modulation. Columns 3 and 4 refer to the oscillator phase and amplitude stability. In addition to this, phase noise of the rf oscillator mixes with the

carrier and rf sidebands in the demodulation process to produce spurious signals in the gravity wave channel. This imposes the limitation on the oscillator phase noise given in column 5, referred to as local oscillator noise. The level of amplitude and frequency stability of the light is achievable but with little tolerance for error in interferometer optics. Requirements on the oscillator assume the reflectivities of the arm cavities for the SRSB are matched to within 1 part in 10^4. Allowing for a modecleaner mistuning of 100 Hz only has a major impact on the 'local oscillator' type noise level, increasing the required frequency stability of the rf source by a factor of 100.

§2.3 Curvature errors and Alignment Fluctuations

For the rf sidebands, the PRC is virtually a degenerate, flat mirror cavity (curvature of the PRM is 10008 m, curvature of the inboard mirrors, 14400 m, $g_1g_2 = 0.997$), highly susceptible to wavefront errors. Any higher order modes, excited either by alignment fluctuations or curvature errors, are also resonant in the PRC, but suffer large diffraction losses. This sets the tolerance to curvature errors of ~5%. This tolerance is at the level of uncertainty in the coating, annealing, and measuring processes for these mirrors.

This is not the case for the carrier. As it is also resonant in the arm cavities it effectively propagates in a stable, non-degenerate cavity ($g_1g_2 = 0.46$). In essence, the stable mode of the arm Fabry-Perot cavity is resonantly coupled to only one of the many modes of the PRC, feeding energy into it. The light in this mode reflected off the arm cavity receives a phase shift of approximately 180 degrees compared to other non arm-cavity resonant modes. Hence when this mode is tuned to resonate in the PRC, all other modes are suppressed as they are near anti-resonant. The impact of this difference between the carrier and the SRSB has the potential to cripple the LIGO detector (see section 2.4).

Slight misalignments couple light out of the TEM_{00} spatial mode into $TEM_{10,01}$ modes. For the carrier field, this produces a relatively static component of TEM_{10} illuminating the detection system. However, as the rf sidebands are only resonant in a degenerate flat mirror cavity, fluctuations in beam pointing couple directly into fluctuations in TEM_{10} rf sideband light leaving the interferometer. These beat with the TEM_{10} mode of the carrier to produce noise in the detection window. This sets the requirements on the alignment sensing and control. Though stringent, these should be achievable with the proposed ASC sub-system.

§2.4 Thermal Lensing

In its initial phase LIGO will be pumped by a 10 W laser with about 6 W incident on the power recycling mirror. The transmission of this mirror, chosen to impedance match the light into the PRC, is on the order of 0.03 (intensity). Specification on the core optics set the absorption in the ITM and BS substrates to be no more than 5 ppm/cm.

Absorption in the ITM induces a spatial variation (transverse and longitudinal) in the refractive index of the glass. The substrate may then act as a lens for the propagating laser beam. This

phenomenon is referred to as thermal lensing. The presence of such a lens may alter the wavefront curvature of the beam. If there are identical lenses in the 2 arms, this will not greatly effect fringe visibility. However, it will mean that the light would no longer be matched to the curvature of the PRM. This will result in a degraded power build up in the PRC.

Extensive FFT modeling has shown that the carrier is NOT subject to these effects. This results from two distinct effects. The first, described earlier, is that any higher order mode generated in the PRC is anti-resonant. The second is that the field propagating back toward the beam splitter from the ITMs is composed of 2 parts: a part which is a direct reflection off the ITM coating, E_d, and the leakage field from the arm cavity, E_l. E_d samples the thermally induced distortion twice picking up a total phase distortion $2\Delta\phi_d$. The leakage field, which is in the mode of the arm cavity, samples the phase distortion only once. Now, as the beam is overcoupled into the arm cavity, the leakage field is approximately twice as large as the directly reflected component, and 180^o out of phase with it. Hence the total reflected field, E_r, is

$$\begin{aligned} E_r &= E_d + E_l \\ &\sim E_{in}[\exp(-2i\,\Delta\phi_d) - 2\exp(-i\,\Delta\phi_d)] \\ &\sim E_{in}[1 - 2i\,\Delta\phi_d - 2 + 2i\,\Delta\phi_d] \\ &= -E_{in}. \end{aligned}$$

Therefore, provided the phase distortion is small, the net result is that the distortion is cancelled! This cancellation, sketched here for ITM transmission distortion, applies quite generally to a perturbative phase distortion occurring *anywhere* in a degenerative cavity which is over coupled to a second (arm) cavity. For example BS distortions are also cured.

However, the rf sidebands in the SRSB scheme are not resonant in the arm cavities. They will therefore be affected by thermal lensing. As the PRC is virtually a flat mirror degenerate cavity for the rf sidebands, such lensing could prove disastrous. Kells has modeled this using the MIT FFT propagation code. Figure 2 plots the total recycling gain for the rf sidebands. For the parameters of LIGO, the ideal (no lensing) gain, $G_{sb.max}$, is about 47 (60 for the carrier). The nominal radius of curvature of the PRM, assuming no thermal lensing, is 10008 m. We see that at the nominal curvature, the inclusion of thermal lensing yields a sideband gain of about 2! This is catastrophic for both interferometer control and for signal extraction. This cannot be compensated by simply increasing the modulation depth.

Fig 2 shows that it is possible to recover most of the circulating power if the curvature of the PRM can be altered. We see that at a curvature of 15000 m the gain is within 15% of the ideal value. Stipulating a minimum sideband gain of 75% of the ideal, the recycling mirror curvature has to be set to within 1000 m of the matching value. Fig 3 shows the effect of a change in input power on a mirror with ROC optimized for 6 W input power. We note that a change of input power of +/- 1 W gives a 10% change in sensitivity, accompanied by a 40% change in the sideband recycling gain. The consequences of this hit in sideband power for the LSC and ASC has not yet been fully explored. It is likely that the Michelson differential mode can still be extracted after signal processing. However, the common mode signals at the pick off and

isolator ports become virtually linearly dependent, *destroying common mode control*.

We note that the optimum mirror curvature is influenced by the mirror absorption and other scattering processes. For example, reducing the absorption by a factor of 2 (to 2.5 ppm/cm), changes the optimum curvature to 12000 m. It is possible that we will not know the absorption to better that a factor of 2. In addition, other scattering processes also influence the optimum curvature. Kells has shown that incorporating such losses can change the optimum curvature by about 15%! We must therefore conclude that it is not possible to predict the power recycling mirror curvature accurately enough. Even if we could, and the PRM was polished for this curvature, it would then have the wrong curvature when light is first introduced presenting a problem for initial lock acquisition.

Adaptive optics, such as variable curvature mirrors would alleviate this. The development of such technology is part of LIGO Advanced R&D but is at least 10 years off implementation.

The problem of thermal lensing of the rf sidebands is the major unknown in the current LIGO design. At best, it will require increasing the modulation depth by about 10%. At worst, it could lead to the breakdown of the entire length control and signal extraction system once the pump power exceeds a critical level. That critical level is not known but it is likely to be not much larger than 6 W. The long term impact on LIGO is a severe restriction on the pump power and therefore on the achievable sensitivity.

§3 The Doubly Resonant Sideband Technique

§3.1 DRSB

In the DRSB technique, the rf sidebands are selected to resonate in both the PRC and the arm cavities, along with the carrier. In this and the next sections we will examine this idea in terms of control signals, frequency and amplitude stability, beam pointing stability and thermal lensing in the ITMs.

For the DRSB method, the nominal lengths are chosen so that both the carrier and the rf sidebands resonate in the arms and the PRC. This is achieved when $L+/2 \sim mc/2f_{mod}$ and $l+ \sim nc/2f_{mod}$, m and n integers. The asymmetry required to couple rf sidebands out at the antisymmetric port for signal extraction is generated by a Michelson asymmetry. After demodulation at the rf frequency, the in phase signals at ports 1 and 2 respond mainly to the arm cavity common mode length fluctuation; the quad phase at ports 1, 2 and 3 mainly to arm cavity differential motions. Michelson common mode and differential mode changes are not dominant at any port. More importantly, the control signals are linearly dependent. As a consequence, DRSBs alone cannot control Michelson length degrees of freedom. This is to be expected since both the carrier and the rf sidebands sense all lengths in the same way. The matrix of discriminants is presented in Table 4. This will be further discussed in section 3.6. Gravity wave signals are still sensed because in effect the dc fields emerging from one arm sense the audio signals from the other arm.

§3.2 DRSB Outcoupling

When the transmission of the power recycling mirror is chosen to maximize carrier build up, it can be shown that maximum transmission of the DRSB sidebands to the antisymmetric port is 50% in power. This can be increased by lowering the PRM reflectivity. For eg, with an asymmetry parameter ($2\pi\Omega\delta$ /c) of 0.42 and PRM mirror reflectivity of 0.9 (amplitude), 90% of the sidebands can be outcoupled. Of course this lowers the carrier buildup. Final choice of parameters will require optimization of sideband power vs carrier power, but is likely to be close to carrier optimization. This is to be compared with the SRSB where in the ideal case, 100% of the sidebands can be outcoupled.

§3.3 Stability Requirements

In this case the rf sidebands also propagate in a coupled cavity which has a pole frequency for the rf sidebands of about 2 Hz. This is higher than the carrier pole frequency due to the Michelson asymmetry used to couple out the sidebands. Therefore noise sidebands on both the carrier and the rf sidebands are strongly filtered above 2 Hz. Table 5 summarizes the stability requirements on the laser and rf oscillator in order for LIGO to achieve a sensitivity of 10^{-20} m. We see the effect of filtering of the rf sidebands in the relaxation of the requirements on the frequency and amplitude stability of the laser and amplitude stability of the rf source by a factor 100 in comparison to the SRSB method (Table 5).

However, the required phase stability of the rf oscillator has increased by a factor of 100. Recall that this noise source arises from the combination of the DC fields on the detector. In the SRSB case, the 'off resonance' reflectivities of the arm cavities are well matched (within 1 part in 10^4). As result the sideband phase shifted leakage field is minimized and this noise source is suppressed. When the sidebands are resonant in the arm cavities this common mode suppression is reduced to about 1 part in 10^2, hence the 100 fold increase in the required oscillator phase stability. At 100 Hz the required phase stability is 10^{-6}. Commercially available oscillators quote -120 dB at 1 kHz. Thus it may require some development to reach the required level. This requirement could be reduced with better arm cavity length fluctuation control and better matching of the arm cavity reflectivities.

Finally, we note the requirement on matching of the arm cavity lengths to resonate the rf sidebands. If the rf sidebands are not exactly resonant with an arm cavity, frequency noise can be converted into output noise. The rf frequency can be adjusted to ensure resonance with 1 of the arm cavities, but only with both cavities if they have matched armlengths. Our analysis shows that this noise mechanism can be ignored (less than 1/10 cf other sources of noise) provided the cavities are matched to within 1 mm. This should be achievable. We suggest a method to set the cavity lengths in section 3.7.

§3.4 Alignment fluctuations

With the rf sidebands resonating in the arm cavities, the PRC will no longer appear as a degenerate flat mirror cavity. The sidebands will have a similar tolerance to beam pointing

fluctuations and curvature errors as the carrier, suppressing alignment induced noise by a factor of ~50 to 100 compared to the SRSB case.

Error tolerance on the radii of curvature of the PRM mirrors can be relaxed to ~ 50%.

§3.5 Thermal lensing

In §2.4 we demonstrated that the carrier is not subject to thermal lensing in the ITMs. By resonating the sidebands in the arm cavities we predict that they should be similarly immune to this distortion. Using the FFT code Kells et al have verified this prediction. In the ideal case (no thermal lensing) the DRSB sideband gain in the PRM is 13 with a Michelson asymmetry of 0.49 m chosen to maximize the outcoupling of the DRSB (50% in power). The radius of curvature of the PRM was set to 10008 m. With the introduction of thermal lensing, the DSRB gain falls less than 3% with DRSB outcoupling remaining at 50%. Changing the radius of curvature by 30% (to 12950 m) has very little impact: the DRSB gain and outcoupling are essentially the same!

It is worth noting that the percentage of light in higher order modes ejected at the main beam splitter is similar for both the DRSB and the SRSB. This reflects the fact that the thermal lenses are assumed equal in both ITMs hence beam splitter interference is not greatly effected. It is the mismatch of curvature onto the PRM that is the problem in the SRSB case.

Clearly, using DRSBs overcomes the sideband thermal lensing problem. In addition, the system is far more stable against geometric errors such as tilts and curvature mismatch. The above results were calculated for a pump power of 6 W. Further work is needed to determine just how much light power can be supported with this arrangement but we expect that a factor of ~10 increase should be sustainable. The use of DRSBs therefore ensures that the initial LIGO will not be limited by thermal effects in the ITMs.

We have not modeled thermal lensing in the beam splitter. However, it is fairly clear that the DRSBs will in general be much more robust against mode re-shaping than SRSBs. For future development of LIGO to higher powers, it is essential that a system robust to thermal lensing be employed.

§3.6 Sensing Michelson lengths

In terms of tolerance to input fluctuations on the laser, thermal lensing and geometric errors, the DRSB technique far surpasses the SRSB method. However, as indicated in §3.2, DRSBs alone cannot sense Michelson lengths. We need to introduce either an SRSB pair or rf sidebands which are not resonant in either cavity. The latter would not allow sensing of the alignment of the ITMs. So to generate error signals for all length degrees of freedom, we propose to use an SRSB pair along with a DRSB pair. This combination also provides the required alignment signals. This does not add an extra pair of sidebands cf the SRSB method as that technique requires the addition of an NRSB pair for alignment sensing.

The SRSB frequency is set by 2 requirements: firstly, it must pass through the modecleaner

and only resonate in the PRC; secondly, the gain in the PRC must be high enough to ensure adequate control signals and system diagonalisation. This second point has a major impact on the choice of SRSB. To sense the Michelson common mode length, the SRSB technique relies on the rate of change of phase of the SRSB reflected off the PRM being large enough so that the contribution of the Michelson common mode to the reflected signal is different to its contribution at the internal pick off signal. Thus the Michelson length change, sensed by the SRSB, dominates the reflected control signal. In our case, the Michelson asymmetry is set by the choice of DRSB. For a DRSB of 19.7 MHz and a typical δ of 0.6 m, the SRSB frequency must be chosen to be 25.5 x DRSB frequency, or 502.35 MHz. The SRSB would for the chosen parameters be impedance matched at 487.36 Mhz. However, this frequency is not resonant in the PRC.

The choice of 502.35 MHz, apart from providing adequate decoupling of the Michelson and arm cavity common modes is close to a dark fringe at the anti symmetric port for the SRSB, minimizing shot noise. We note that if the SRSB was exactly at a dark fringe we would lose a signal for controlling the Michelson differential mode. The choice of 502.35 MHz is therefore near optimum for the fiducial interferometer based on LIGO specifications.

Table 6 displays the total length control plant. These results are obtained assuming: carrier is impedance matched; δ is chosen to maximize DRSB output; frequencies of the DRSB and SRSB selected for appropriate resonances, modecleaner transmission, sideband gain in the PRC and minimization of interference due to sideband beats.

We have not included the influence of thermal lensing on the SRSB control plant. Its major impact will be on the common mode diagonality. However, as we begin with the SRSB being overcoupled, these sidebands can suffer a reasonable amount of loss before common mode distinction is lost. In regard to the differential modes, signal processing may be required, however the extra noise filtering of the DRSB reduces the requirements on l- control. The important point here is that if interferometer control is compromised with this SRSB, a system based purely on SRSB will have catastrophically failed.

The major question is whether we can detect at such a high frequency with sufficient SNR. This frequency is only used for auxiliary length sensing and not gravity wave signal extraction. Photodetectors with quantum efficiency of around 90% and optical power separation of about 250 μW (NEP of 8 pW/Hz) are readily achievable (for eg, the ETX-300 MMIC2170). Further work is needed to determine the exact requirements but properly designed electronics should ensure successful operation at such high frequencies.

If required the SRSB frequency can be lowered by increasing the asymmetry and changing the DRSB frequency. Within the current LIGO space limitations, the best that could be achieved would be halving the frequency to around 250 MHz.

Alternatively, the SRSB frequency could be chosen to be smaller than the DRSB frequency. For example, if the DRSB is set at 49.128 MHz, the SRSB frequency could be set to 24.564 MHz, 1/2 the DRSB. This would prove a convenient choice in terms of SRSB gain. However, the second harmonic of the SRSB would coincide with the DRSB and intermodulation products

may prove disastrous. In addition, the antisymmetric port would be close to a bright fringe for the SRSB. Nevertheless such a choice warrants further investigation.

Other schemes for length control

Other length control schemes are possible. For example, by resonating the DRSB in only one arm cavity, the advantages of the stable coupled cavity may be preserved but as the symmetry of the DRSB and carrier is broken, access to Michelson control may be achieved. This arrangement also provides temporal filtering to the rf sidebands. Another possibility may be to resonate 2 different sideband frequencies, one in either arm.

§3.7 Setting the arm cavity lengths

It is possible to mimic the Michelson asymmetry by deliberately detuning the rf sidebands from resonance . The total effective length asymmetry would then be given by

$$\delta_{eff} = \delta + G_{FP} * L-$$

where G_{FP} is the arm cavity gain and L- is the absolute difference in length between the arm cavities. Note L- can be positive or negative. For example, standard LIGO arm cavities have a gain of about 130, hence an arm cavity length difference of 4.6 mm is required to mimic a δ of 0.6 m. However, we noted in §3.3 that in order to avoid converting frequency noise on the rf sidebands into a significant amount of intensity noise, the arm cavities had to be matched to better than 1 mm. Thus using an arm cavity offset to generate the asymmetry is not viable.

Therefore, to avoid confusion with a Michelson length asymmetry we need to ensure that the arm cavities are matched to better than $0.1*\delta/G_{Fp}$. Taking an asymmetry of between 0.4 m and 0.6 m this means matching to better than about 400 μm.

We propose to achieve this in a number of stages. Firstly, the arm cavity lengths will be set by GPS, reaching a matching of about 1 cm. Next, we can use the spatial beat length between the carrier and rf sidebands reflected off each cavity (*a la* Malik et al.) to measure that cavity length to order 100 μm and then adjust the stacks so that sideband resonance is obtained. Finally, after achieving lock, we will apply a small frequency modulation (a factor 10 above residual) at about 5 Hz to the input laser field and by demodulating the light transmitted by each cavity, monitor the length offset from sideband resonance. (The long arm cavity length gives a large frequency to phase conversion, which leaves a common mode demodulated signal on the transmitted light about ~100 times above shot noise for a length deviation of 1 mm.) The LSC control will keep the arm lengths the same; the monitor signal will give common stack (or frequency) feedback to keep the sidebands on resonance. Thus by feeding back to the test masses via the stack actuators we estimate that it should be possible to match the arm cavity lengths to the sideband frequency to better than 100 μm.

Conclusions

The use of sidebands resonant only in the power recycling cavity presents serious short and longer term problems for interferometer control and signal extraction. These problems arise from sideband spatial instability due to a combination of thermal lensing and propagation in a degenerate cavity. Rf sidebands which are resonant in both the power recycling cavity and the arm cavities, as is the carrier field, do not suffer from these afflictions. In addition they pick up a high degree of temporal filtering.

Due to linear dependence of the control plant for the pure DRSB, control of interferometer auxiliary lengths will still require the use of an SRSB pair and hence careful choice of mirror parameters. However, signal extraction is achieved using the highly robust DRSB rf field. This allows constraints on laser frequency and intensity noise to be relaxed or, more importantly, *constraints on differential length control to be relaxed.* Hence the impact of thermal lensing of SRSBs used for auxiliary control is much less significant than is the case when the SRSBs are also used for signal extraction. The result of this is that the system can be pushed to higher pump powers, and hence better sensitivity, before breakdown occurs.

Ideally, we would like a system in which all sidebands are robust to thermal distortions. The use of rf sidebands resonant in 1 arm cavity and not the other may provide such a system, and warrants deeper investigation.

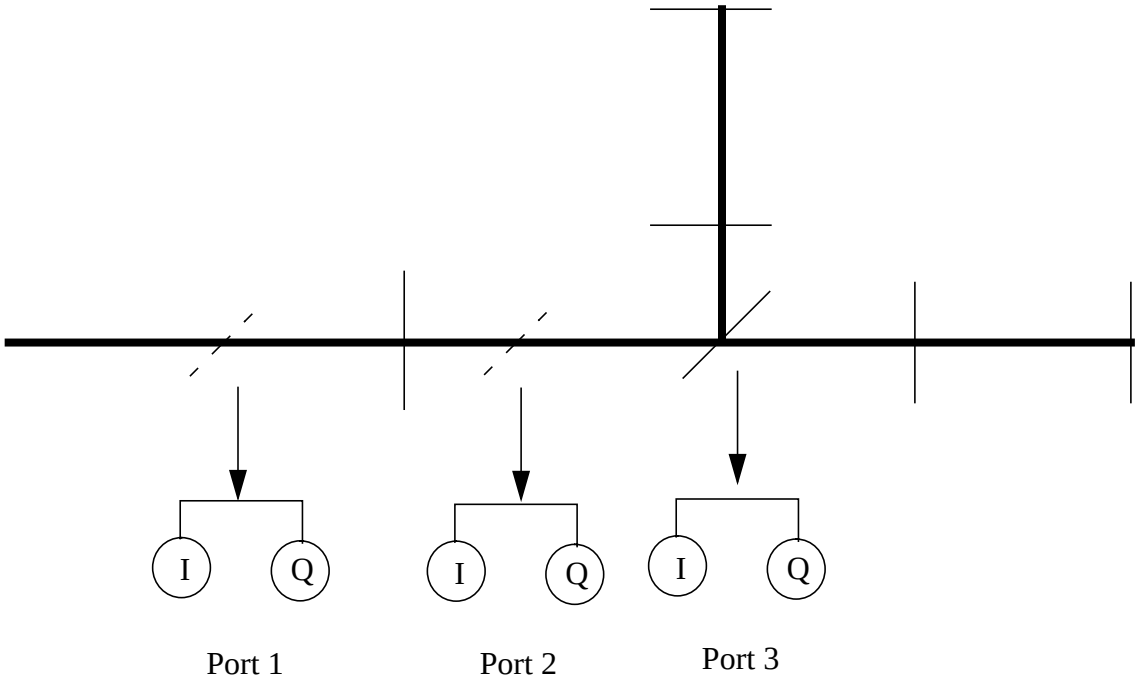

Figure 1: Schematic layout of LIGO interferometer

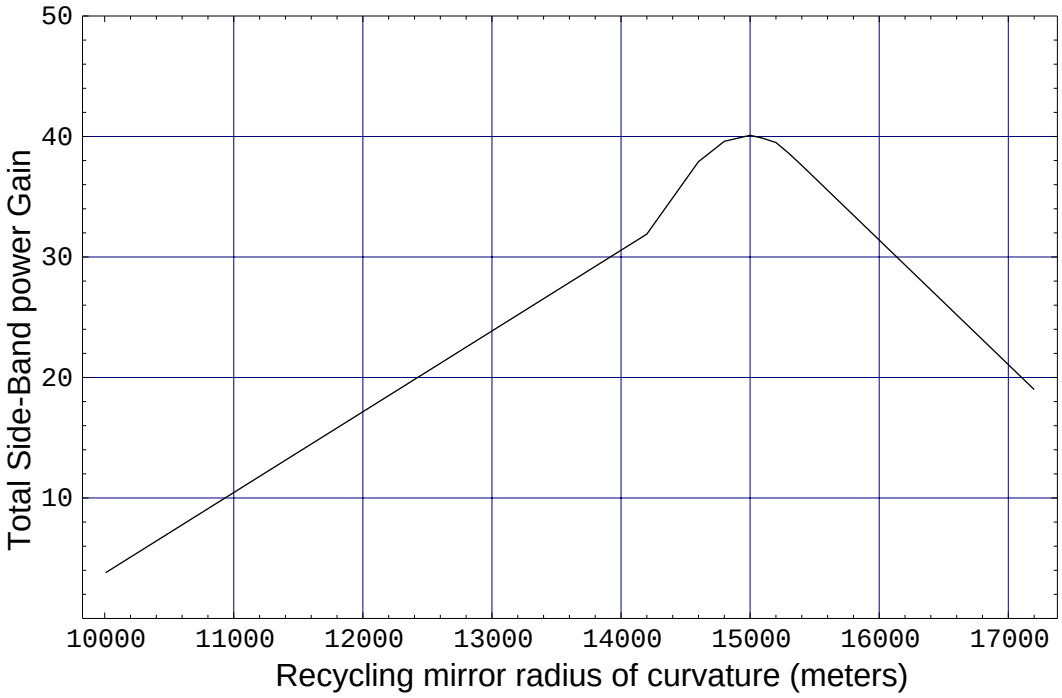

Figure 2: SB gain for optimal Recycling Mirror ROC of 15 km

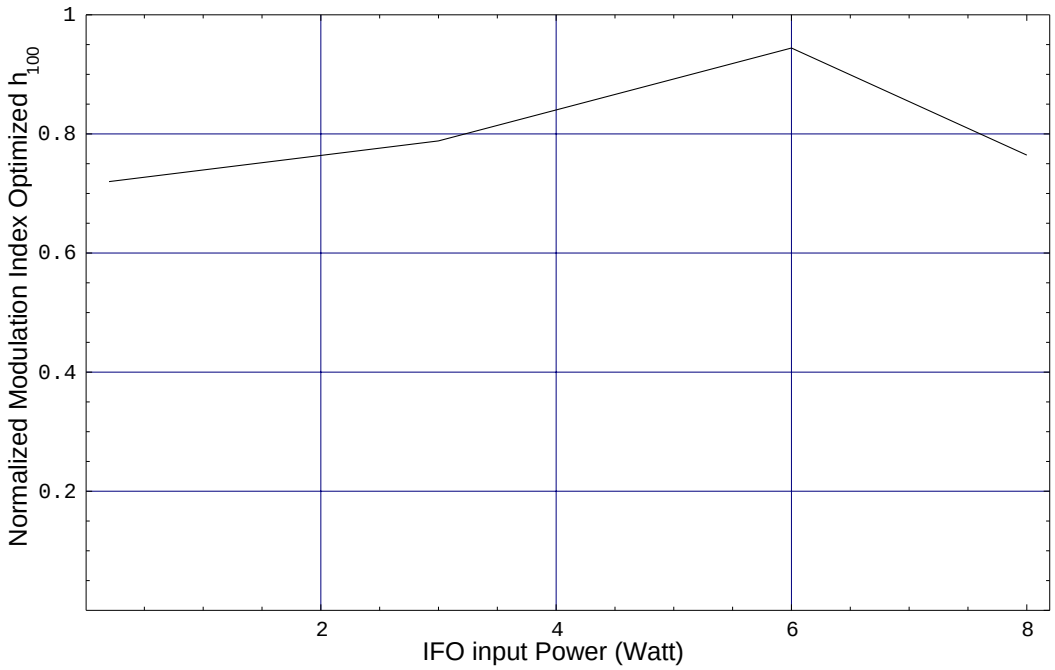

Figure 3: IFO sensitivity

Table 2: SRSB Matrix of Discriminants (f = 24 MHz)

	$d\Phi_+$	$d\phi_+$
dV_1	-1	-0.001
dV_2	-1	+0.0007
	$d\Phi_-$	$d\phi_-$
dV_2	0.0076	1
dV_3	-1	-0.0076

Table 3: Stability Requirements (/radish) on SRSB at 100 Hz[a] (f = 24 MHz)

Laser		Oscillator		LO
Freq	Amp	Phase	Amp	Phase
2×10^{-7}	2×10^{-8}	-90 dBc	2×10^{-8}	-80 dBc[b] -120 dBc[c]

a. assumes $dL_- = 10^{-13}$ m
b. assumes sideband exact resonance in mode cleaner
c. assumes sideband detune from mode cleaner of 100 Hz

Table 4: DRSB Matrix of Discriminants

	$d\Phi_+$	$d\phi_+$
dV_1	-1	-0.0076
dV_2	1	+0.0076
	$d\Phi_-$	$d\phi_-$
dV_2	1	0.0076
dV_3	-1	-0.0076

Because of the linear dependence of the mixer signals we cannot extract Michelson d.o.f.

Table 5: Stability Requirements (/radish) on DRSB at 100 Hz[a] (f = 19.7 MHz)

Laser		Oscillator		LO
Freq	Amp	Phase	Amp	Phase
1×10^{-5}	1×10^{-6}	-84 dBc	1×10^{-6}	-120 dBc[b]

a. assumes $dL_- = 10^{-13}$ m

b. assumes sideband exact resonance in mode cleaner; not greatly changed by 100 Hz MC detuning.

Table 6: DRSB Matrix of Discriminants with f_D= 19.7 MHz, f_S = 502.35 MHz

	$d\Phi_+$	$d\phi_+$
dV_1^S	-1	-0.004
dV_2^S	-1	+0.006
dV_1^D	1	0.0076
dV_2^D	-1	-0.0076
	$d\Phi_-$	$d\phi_-$
dV_2^S	0.0076	1
dV_3^S	-1	-0.0076
dV_2^D	1	0.0076
dV_3^D	-1	-0.0076

This matrix yields linear independence of the arm and Michelson d.o.f.